



HAL
open science

Electronic structure, elastic and optical properties of $\text{Bi}_2\text{Te}_3/\text{Sb}(2)\text{Te}_3$ thermoelectric composites in the periodic-superlattice thin films

Jia Fu, Jiaxuan Huang, Fabrice Bernard

► **To cite this version:**

Jia Fu, Jiaxuan Huang, Fabrice Bernard. Electronic structure, elastic and optical properties of $\text{Bi}_2\text{Te}_3/\text{Sb}(2)\text{Te}_3$ thermoelectric composites in the periodic-superlattice thin films. *Composites Communications*, 2021, 28, 10.1016/j.coco.2021.100917 . hal-03414216

HAL Id: hal-03414216

<https://hal.science/hal-03414216>

Submitted on 16 Oct 2023

HAL is a multi-disciplinary open access archive for the deposit and dissemination of scientific research documents, whether they are published or not. The documents may come from teaching and research institutions in France or abroad, or from public or private research centers.

L'archive ouverte pluridisciplinaire **HAL**, est destinée au dépôt et à la diffusion de documents scientifiques de niveau recherche, publiés ou non, émanant des établissements d'enseignement et de recherche français ou étrangers, des laboratoires publics ou privés.



Distributed under a Creative Commons Attribution - NonCommercial 4.0 International License

Electronic structure, elastic and optical properties of Bi₂Te₃/Sb₂Te₃ thermoelectric composites in the periodic-superlattice thin films

Jia Fu^{1,2*}, Jiakuan Huang¹, Fabrice Bernard²

¹School of materials science and engineering, Xi'an Shiyou University, Xi'an, Shaanxi, 710065, China

²Matériaux, thermo-rhéologie (MTRHEO), LGCGM, Institut national des sciences appliquées de Rennes, Rennes-35708, France

*Corresponding author's e-mail: fujia@xsyu.edu.cn

Abstract: The outstanding p-type Sb₂Te₃-based materials such as the Bi₂Te₃/Sb₂Te₃ thermoelectric thin films with consideration of anisotropy and synergetic optimization of thermoelectric performance are promising used in practical applications through improving the power factor and reducing the thermal conductivity. Electronic structure, heat capacity and homogenized elastic properties of anisotropic Bi₂Te₃ and Sb₂Te₃ crystals are investigated, and then modeled to calculate elastic properties of the composite Bi₂Te₃/Sb₂Te₃ thin films. Debye temperature, thermal conductivity and *ZT* value are especially analysed and found that the Sb-5p/Bi-6p and Te-5p at Debye temperatures of 179.29 K and 178.20 K, with the energy gap of 0.207 eV and 0.256 eV in Bi₂Te₃ and Sb₂Te₃, which contribute a multiscale modeling scheme from periodic single crystal film to multilayer composite Bi₂Te₃/Sb₂Te₃ thin films with higher *ZT* value, resulting in the significant reduction of band gap and the thermal conductivity due to its superlattice multi-layer structure.

Keywords: Composite Bi₂Te₃/Sb₂Te₃ structure; Debye temperatures; Homogenized elastic properties; Thermoelectrics;

1. Introduction

Based on Seebeck effect and Peltier effect, thermoelectric (TE) materials to realize the conversion between thermal energy and electrical energy are milestone materials in the thermal power generation, solid state refrigeration, wireless sensing, smart device and high-performance optoelectronic device [1-6]. The bismuth telluride (Bi₂Te₃) and antimony telluride (Sb₂Te₃) in high-quality Bi₂Te₃/Sb₂Te₃-based TE materials are obligatory in photodiodes, sensors, thermoelectric generators, thermal generator or solid-state cooling devices [7-10]. The performance of thermoelectric materials is generally measured by a dimensionless value (*ZT*) from the formulas: $ZT = S^2 \cdot \sigma \cdot T / \kappa$, where, *S* is the Seebeck coefficient, σ is the conductivity, *T* is the absolute temperature, $S^2 \cdot \sigma$ is power factor (*PF*), κ is the thermal conductivity ($\kappa = \kappa_e + \kappa_L$). The κ is consisted of the carrier thermal conductivity κ_e and lattice thermal conductivity κ_L , which can be improved between thermoelectric and mechanical performances in polycarbonate/single-walled carbon nanotube composite films [10]. The potential inorganic semiconductor material is still Bi₂Te₃/Sb₂Te₃ compounds [7, 8]. Except for the Bi₂Te₃ and Sb₂Te₃ strong topological insulators, (Bi₂Te₃)_x(Bi₂Se₃)_{1-x} and Sb₂(Te_{1-x}Se_x)₃ with higher high *ZT* value from 1.0-2.0 are discovered as the important milestones [9-13], with the research methods like DFT method [12, 14], heat pulse method [13], X-ray powder diffraction [14, 15] etc.

In the present case of thermoelectric compounds of Sb₂Te₃ and Bi₂Te₃, few reports of theory is available on electronic structure, thermoelectric or mechanical properties [9-15,16]. The Bi₂Te₃ alloy is reported by using molecular epitaxy to prepare Bi₂Te₃ superlattice materials [17] and the thermoelectric compounds later are extended to Bi-Se-Te ternary alloys [18, 19]. For Bi₂Te₃ alloy, the electronic structure

has been described [20] and the mechanical properties coupling the obtained elastic constant C_{ij} are especially investigated from the first-principle calculation [20, 21]. The p-type Bi_2Te_3 - Sb_2Te_3 single crystal synthesised in experiment by the moving heating method, with a PF value upper to $5.3 \times 10^{-3} \text{ W}/(\text{K}^2 \cdot \text{m})$ [4], which is 67.9 % higher than that of Bi_2Te_3 alloy. Sb_2Te_3 -based films can be prepared by thermal evaporation [4, 7], sputtering [18], electrochemical deposition [5], molecular beam epitaxy, pulsed laser deposition (PLD) [6, 13], MBE deposition [23] and chemical vapor deposition (CVD) techniques [24], with the ZT region of 0.40-1.75 and the PF region of 1.32-4.30 [4-7, 13, 18], separately. Among the thermoelectric Sb_2Te_3 -based thin films materials studied at present, Bi-Te semiconductor with a ZT about 1 and the conversion efficiency less than 10.0 %, which is far from satisfactory [1-3]. In particular, micro thermoelectric devices based on thermoelectric Sb_2Te_3 -based films especially for the composite $(\text{Bi}_2\text{Te}_3)_x(\text{Sb}_2\text{Te}_3)_{1-x}$ films greatly depends on these two layered hexahedral structure with $\bar{R}3m$ space group and their synergetic optimization combination [24-27]. Therefore, Sb atom is added to replace Bi in Bi_2Te_3 to form solid solution on the basis of the Bi-Te binary alloy, so as to change the carrier type and density of the p-type Sb_2Te_3 semiconductor (band-gap $E_g < 0.3 \text{ eV}$) [28] and improve the doping properties of p-type Sb_2Te_3 -based thin films. It is therefore necessary to study the mechanical stability, Debye temperature, and band gap of Sb_2Te_3 , Bi_2Te_3 and composite $\text{Sb}_2\text{Te}_3/\text{Bi}_2\text{Te}_3$ superlattice structure, separately.

By reviewing the references, due to their highly complex band structures and broadband wavelengths, some basic physical properties of Bi_2Te_3 and Sb_2Te_3 of TE layered semiconductor materials still remain unexplored, especially for understanding their strong optical absorbance and the narrow direct band gap of $\text{Bi}_2\text{Te}_3/\text{Sb}_2\text{Te}_3$ -based TE materials. However, the detailed thermodynamic parameters, Debye temperature, heat capacity and the homogenized elastic properties of anisotropic Bi_2Te_3 , Sb_2Te_3 and Bi_2Te_3 - Sb_2Te_3 crystal structures remain scarce and far way from obtaining an agreement. Through the systematical research on the based ground elastic constants C_{ij} , elastic moduli, Debye temperature, Young's modulus and Poisson ratios of hexagonal Sb_2Te_3 and Bi_2Te_3 single crystal, this work provides a theoretical basis to investigate the surface adsorption and doping on Bi_2Te_3 and Sb_2Te_3 thin film of $(\text{Bi}_2\text{Te}_3)_x(\text{Bi}_2\text{Se}_3)_{1-x}$, $\text{Sb}_2(\text{Te}_{1-x}\text{Se}_x)_3$, $\text{Bi}_2\text{Te}_{2.7}\text{Se}_{0.3}$ and $\text{Bi}_{0.46}\text{Sb}_{1.54}\text{Te}_3$ with higher ZT value or composite p-type Bi_2Te_3 - Sb_2Te_3 - Bi_2Te_3 - thin films, aiming to the exploitation of the multiscale modeling and physical properties in calculation of the meaningful p-type Sb_2Te_3 -based thin film materials. Due to the anisotropy of single crystal, the simulation of thin film materials is more complicated. By optimizing the band structure of nano-composite structures, the density of states near Fermi energy levels and phonon scattering can be increased, and the synergistic optimization of thermoelectric properties with higher ZT value can be fatherly realized in future.

2. Modeling and computational approach

2.1 Modeling of Sb_2Te_3 , Bi_2Te_3 and p-type Bi_2Te_3 - Sb_2Te_3 - structures

Sb_2Te_3 and Bi_2Te_3 belongs to the hexagonal $\bar{R}3m$ coordinate system ($\alpha=\beta= 90^\circ$, $\gamma= 120^\circ$, No.166) [3, 12, 27-29] with a periodic layered structure unit consists of five atomic layers along the C-axis. The order arranges alternately in a cycle of Te(I)-Bi/Sb-Te(II)-Bi/Sb-Te(I), where Te(I) is connected with Bi/Sb by covalent bond and ionic bond, and Te(II) is connected with Bi/Sb by covalent bond, adjacent Te(I) and Te(I) are connected by the van der Waals bond [27-29]. The interaction between Te and Te of two adjacent crystal plane atomic layers is relatively small. Modeling of Sb_2Te_3 , Bi_2Te_3 and p-type Bi_2Te_3 - Sb_2Te_3 - structures are shown in Fig.1.

From Fig.1 (a), the primitive cells of Sb_2Te_3 and Bi_2Te_3 and contain three Layer Quintuple Layer (QL) elements, each of which consists of two Sb/Bi atomic layers and three Te atomic layers. Lattice parameters a and c of Sb_2Te_3 and Bi_2Te_3 are 4.269Å, 30.465Å and 4.384Å, 30.488Å, which are close to references[15, 25, 27-29] of Sb_2Te_3 and references[9, 15, 26-28] of Bi_2Te_3 . The volumes of Sb_2Te_3 and Bi_2Te_3 are

480.82Å³ and 507.46 Å³, which are close to references [15, 29] of Sb₂Te₃ and reference [15] of Bi₂Te₃. Based on the crystals of Sb₂Te₃ and Bi₂Te₃, a vacuum layer of approximately 15Å was constructed to obtain the surface lattice structure, and a silicon substrate length about 6Å was added to the calculation, resulting in a surface structure of 1 to 6 units of QL layer, with the periodic superlattice model of composite ply-type -Bi₂Te₃-Sb₂Te₃- structures is established in Fig.1(b), in order to keep consistent with the super lattice thin film model of composite ply-type -Bi₂Te₃-Sb₂Te₃- thin film structures in Fig.1(c) of high-thermoelectric performance considering size effect at nanoscale [30-32].

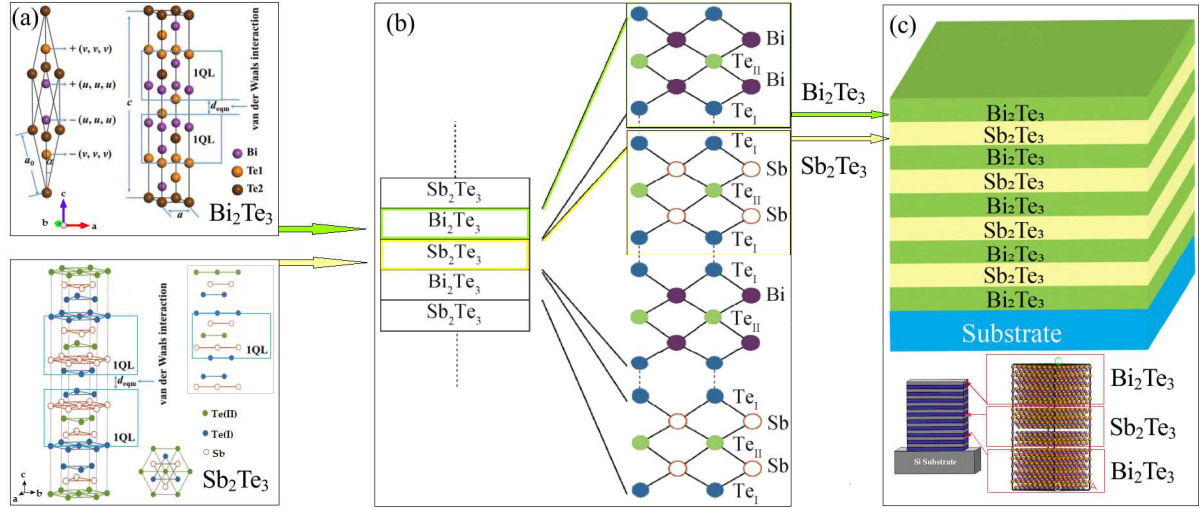


Fig.1 Modeling of Sb₂Te₃, Bi₂Te₃ and ply-type -Bi₂Te₃-Sb₂Te₃- structures: (a) Crystal structure of Bi₂Te₃ and Sb₂Te₃; (b) Synthesis of Bi₂Te₃/Sb₂Te₃ superlattice; (c) Schematic diagram of the crystal structure of the Bi₂Te₃/Sb₂Te₃ superlattice.

2.2 Computational approach

The Perdew-Burke-Ernzerhof (PBE) and mBJ (modified Becke-Johnson potential) functions by generalized gradient approximation (GGA) were adopted as the exchange-correlation potential [12, 29]. The ultra soft pseudopotential was used to deal with the interaction between real ion and valence electron, and plane wave basis was set to describe the wave function of the system electron. The $4 \times 4 \times 4$ k-point mesh for Sb₂Te₃ and Bi₂Te₃ was used in the self-consistent field. The plane-wave basis set cut off energy E_{cut} was 300 eV. The mechanical properties and Debye temperature with considering experimental parameters of Sb₂Te₃ and Bi₂Te₃ structures [33-35, 36] were calculated accordingly.

3. Results and discussion

3.1 Lattice parameters, electronic structure and density of state (DOS)

Variation of lattice parameters under various temperatures, electronic band structures and DOS of Sb₂Te₃ and Bi₂Te₃ thermoelectric compounds are shown in Fig.2.

From Fig.2 (a), with the increase of temperature, the lattice parameters increased. It can be seen from Fig.2 (b) that the C_V value gradually reaches to the Dulong–petit limit $3n \cdot N_A \cdot K_B$, which is close to the other reference [9, 11]. Unlike the temperature, the pressure has little effect on the C_p and C_V [45]. From Fig. 2 (c), the calculated total DOS display the place that the conduction band and the low lying valence band contributed by s and p orbital states. The DOS of the Fermi level is slightly greater than zero, indicating the weak metallic properties. The total DOS of Sb₂Te₃ and Bi₂Te₃ in the range of 15 ~ -6 eV and 15 ~ -7 eV are mainly composed of Sb-5s/Bi-6s and Te-5s states, while in the range of -6 ~ 0 eV and -7 ~ 0 eV composed of Sb-5p/Bi-6p and Te-5p. Above the Fermi level, the total DOS is mainly consists of Sb-5p/Bi-6p, Te-5s

and Te-5p states. Since, Sb and Bi with p-electron bind in an ionic fashion with the neighbouring Te-p orbitals in Sb_2Te_3 and Bi_2Te_3 molecules. For the conduction band of Bi_2Te_3 , the contribution of Bi-6p state is larger, and for the valence band, the contribution of Te(I)-p state is larger. The Te(II)-5p has a smaller contribution to the conduction band and valence band near the Fermi level. The electronic structures and DOS calculated by PBE-GGA along the direction of high symmetry points in the Brillion zone are shown in in Fig. 2(d), showing that the small direct bandgap are 0.207 eV for Sb_2Te_3 and 0.256 eV for Bi_2Te_3 .

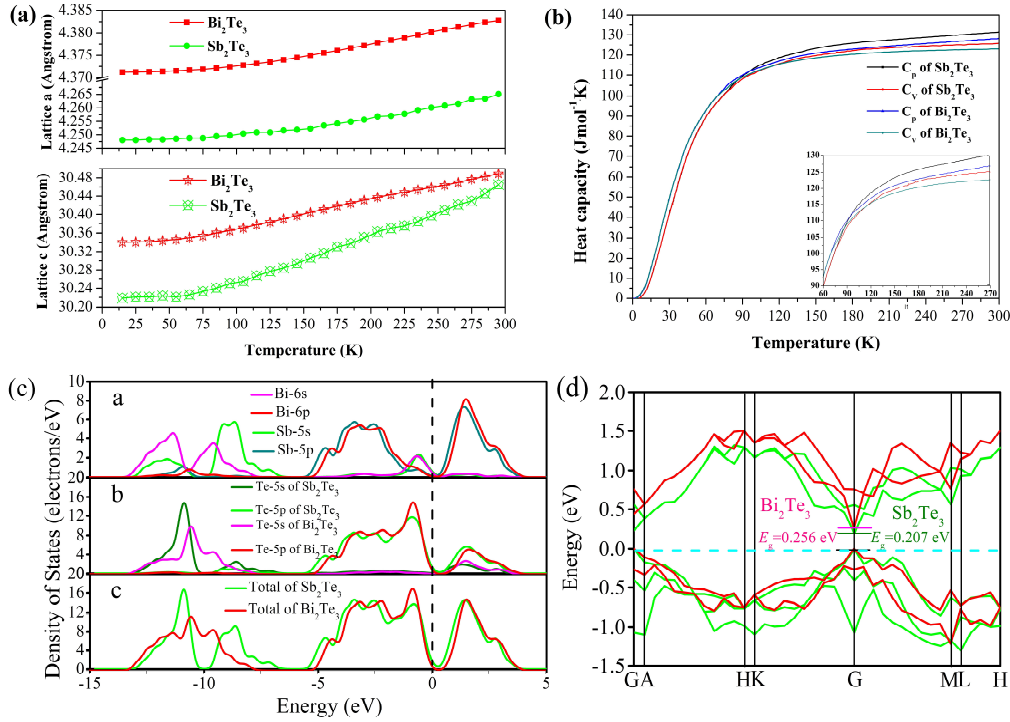


Fig.2 Lattice parameters, heat capacity, electronic band structures and DOS of Sb_2Te_3 and Bi_2Te_3 thermoelectric compounds: (a) Lattice parameters of Bi_2Te_3 and Sb_2Te_3 ; (b) Heat capacity of $\text{Bi}_2\text{Te}_3/\text{Sb}_2\text{Te}_3$; (c) Electronic band structures of $\text{Bi}_2\text{Te}_3/\text{Sb}_2\text{Te}_3$; (d) DOS of Sb_2Te_3 and Bi_2Te_3 .

3.2 Optical properties comparison of single Sb_2Te_3 and Bi_2Te_3 crystals

The optical constants such as absorption, reflectivity, energy loss function, refractive index, conductivity, dielectric function, are shown in Fig. 3.

The optical absorption in Fig. 3 (a) that the peak of the absorption region is at 3.0 eV. In the range of photon energy greater than 18.0 eV, the absorption spectrum of Sb_2Te_3 and Bi_2Te_3 tends to zero, indicating that there is no absorption peak. The main reflection at sharp peak in Fig. 3 (b) occurs at 8.5 eV and 9.0 eV, and the reflectivity of the material is extremely high. The crystal has a higher resistivity in the energy region of 3.0-10.0 eV and 3.0-9.0 eV. Besides, the maximum loss function peak of Sb_2Te_3 and Bi_2Te_3 appears at 11.5 eV and 10.5 eV in Fig. 3 (c). The refractive index $n(\omega)$ of Sb_2Te_3 and Bi_2Te_3 at 0 eV is calculated to be 7.0 and 6.0, and their main peak appears both at 1.5 eV, but the corresponding refractive index is about 7.5 and 6.8, separately. Sb_2Te_3 and Bi_2Te_3 have both a light refraction characteristic of 0~1.5 eV far greater than their absorption characteristic. The static value $n(0)$ at 0eV for Sb_2Te_3 is 7.13 and 6.18 for Bi_2Te_3 . From the optical conductivity in Fig. 3 (e), there is an obvious peak at 2.0 eV with the value of 11fs^{-1} . There is also a weak peak at 13.0 eV. From Fig. 3(d) to Fig. 3(f), the spectral characteristics $n(\omega)$ are identical to the dielectric function $\epsilon_1(\omega)$. In Fig. 3(f), for the Sb_2Te_3 and Bi_2Te_3 at 0 eV, the real part of the dielectric function (ϵ_1) corresponds to a static dielectric constant of about 48.0 and 37.0. The imaginary part of the dielectric function has a peak (2.5 eV and 2.0 eV), and ϵ_2 is about 56.0 and 50.0. These differences can be attributed to the common transition of Sb-5s/Bi-6p and Te-5s between the conduction band and the

valence band. The static dielectric constant $\epsilon_1(0)$ is parallel to the static refractive index $n(0)$.

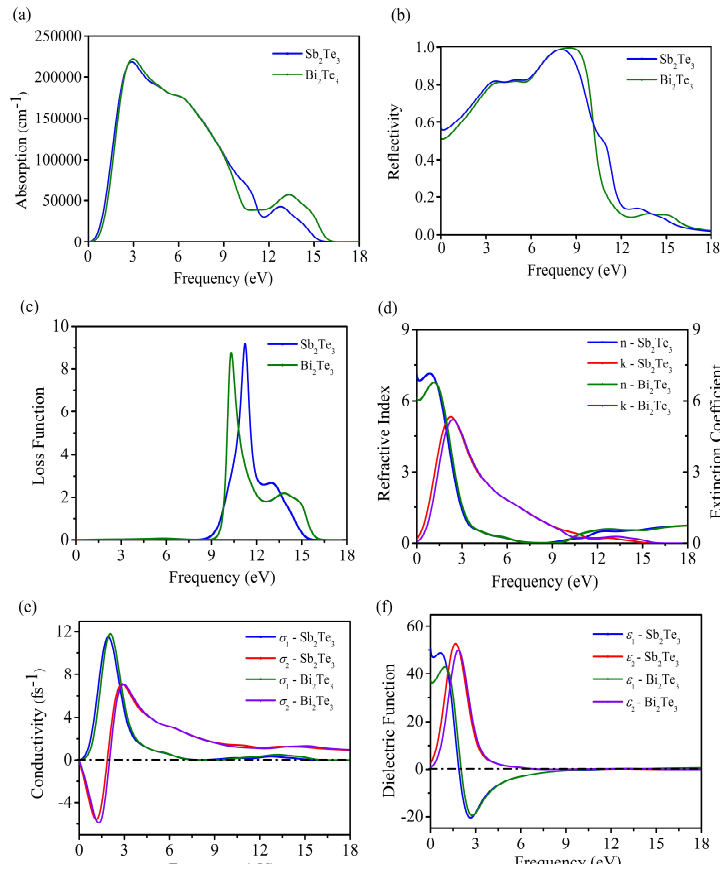


Fig. 3 Calculated optical properties of Sb₂Te₃ and Bi₂Te₃ from 0 to 18 eV. (a) Absorption coefficient (b) optical reflectivity (c) electron energy loss function (d) refractive index and extinction coefficient (e) optical conductivity and (f) dielectric function constant

As the exact band gaps of Sb₂Te₃ and Bi₂Te₃ remain many controversies [46], it is necessary to study the optical properties, anisotropy and precise band gap, due to the little difference between the experimental Seebeck coefficient S of Bi_{2-x}Sb_xTe₃ and the calculated S of Sb₂Te₃ [46], to better understand the mechanical properties of the Sb₂Te₃/Bi₂Te₃ superlattice thin films considering thin film thickness.

3.3 Anisotropy of single crystal and homogenization of polycrystals

The calculated elastic constants C_{ij} of Sb₂Te₃ ($C_{11}=70.52$ GPa, $C_{12}=15.38$ GPa, $C_{13}=25.13$ GPa, $C_{33}=48.16$ GPa, $C_{44}=22.87$ GPa) and Bi₂Te₃ ($C_{11}=72.11$ GPa, $C_{12}=12.69$ GPa, $C_{13}=28.25$ GPa, $C_{33}=50.35$ GPa, $C_{44}=28.78$ GPa) are close to other Sb₂Te₃ reference [29] and Bi₂Te₃ references [9, 11, 25], which are all satisfied with the Born's stability restriction relations [29, 37, 38], indicating that the modeled crystals are stable in mechanical mechanics. Based on the definition of Reuss and Voigt bounds, Y-parameter estimation method containing hexagonal crystal surface normal [49] is used for the comparative study the homogenization of polycrystals, exhibiting the anisotropy of elastic moduli in function of the orientation of the crystal plane. Surface construction of bulk, shear and Young's moduli of Sb₂Te₃ and Bi₂Te₃ are in Fig. 4.

Based on the elastic constants C_{ij} , the Debye temperature [29, 38] and homogenized elastic moduli can be estimated based on the Voigt-Reuss-Hill estimation [40]. The Bulk modulus B , shear modulus G and Young's modulus E are 35.39GPa, 22.12GPa and 54.91GPa for Sb₂Te₃, in comparison of 36.94GPa, 59.75GPa and 24.28GPa for Bi₂Te₃, which are close to reference [29] of Sb₂Te₃ and reference [25] of Bi₂Te₃. Young's modulus in x/y -direction ($E_{x/y}$) and that in z -direction (E_z) are 57.32GPa and 33.46GPa for Sb₂Te₃. The $E_{x/y}$ and E_z of Bi₂Te₃ are 56.08GPa and 31.53GPa, which is close to references [9, 25]. The

B/G ratios of Sb_2Te_3 and Bi_2Te_3 are 1.521 and 1.600, less than the critical value 1.75 proposed by Pugh's criterion, showing that toughness is relatively small [38]. The higher E is, the more covalence enhances and the less ductile character is [47, 48]. Besides, Bi_2Te_3 is more covalent than Sb_2Te_3 and shows less ductile character than Sb_2Te_3 by Pugh's ratios. From Zener's anisotropy factor, Bi_2Te_3 is less isotropic than Sb_2Te_3 and may bring in cracks or microstructure defects [38]. Therefore, Poisson's ratio of 0.24 for Sb_2Te_3 is more resistant than 0.23 for Bi_2Te_3 , with a certain character of fracture resistance [37, 38].

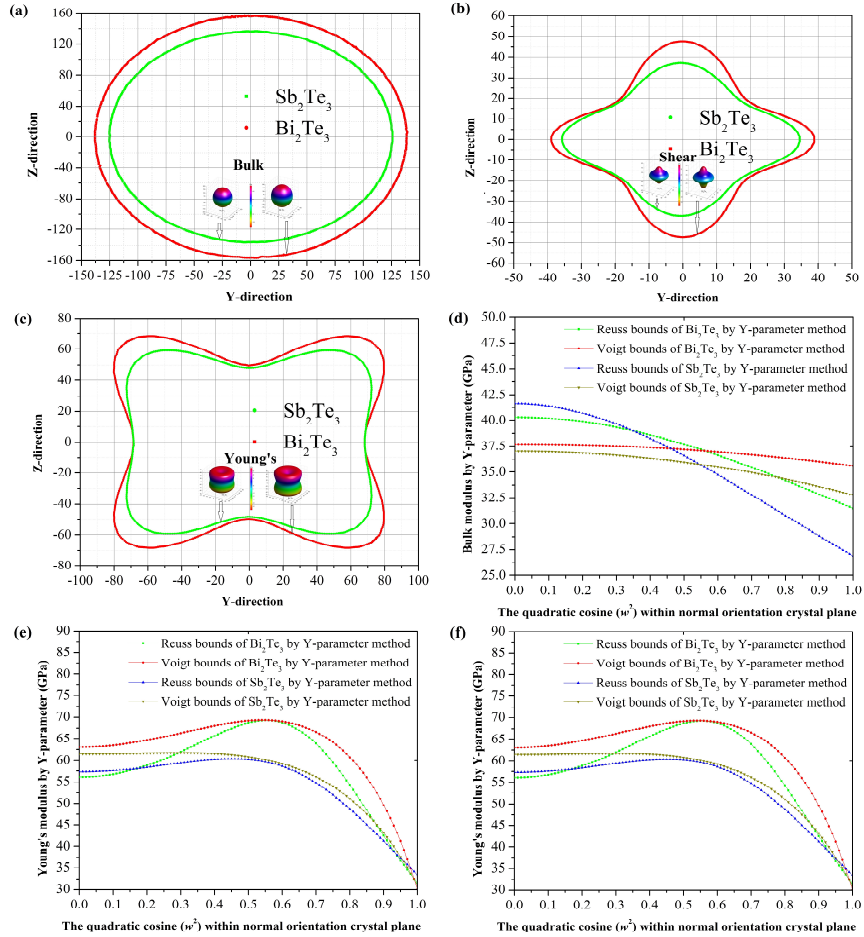


Fig. 4 Construction and Y-parameter evaluation of bulk, shear and Young's moduli of Sb_2Te_3 and Bi_2Te_3 polycrystals: (a) Bulk modulus construction; (b) Shear modulus construction; (c) Young's modulus construction; (d) Shear modulus by Y-parameter estimation; (e) Shear modulus by Y-parameter estimation; (f) Young's modulus by Y-parameter estimation.

Relationship between elastic moduli and plane orientations for Sb_2Te_3 and Bi_2Te_3 by Reuss and Voigt bounds in Fig. 4(a)-(c) shows that the bulk, shear and Young's moduli are anisotropic. Young's modulus of Sb_2Te_3 and Bi_2Te_3 has a significant deviation in shape from the sphere, indicating a great anisotropy. Fig. 4(a)-(c) point out the three-dimension projection curve, and there is little change on the surface of bulk modulus curves, with the outer curve of Bi_2Te_3 and inner curve of Sb_2Te_3 , which is in accord with the A^U value of Sb_2Te_3 and Bi_2Te_3 (are greater than zero and deviates to zero), indicating that Sb_2Te_3 and Bi_2Te_3 have high anisotropic mechanical properties. From Fig. 4(d) to Fig. 3(f), Young's modulus of Sb_2Te_3 and Bi_2Te_3 using various GGA-PBE methods is between 31.04-69.25 GPa for Bi_2Te_3 and 30.93-61.74 GPa Sb_2Te_3 of the Reuss and Voigt bounds in function of the crystal plane orientation. It can be also seen that shear modulus of Sb_2Te_3 and Bi_2Te_3 by Reuss and Voigt bounds of Y-parameter is between 11.82-29.13 GPa for Bi_2Te_3 and 11.94-25.32 GPa for Sb_2Te_3 . Moreover, the comparison of Young's modulus and shear modulus of Sb_2Te_3 and Bi_2Te_3 are very close to each other.

Furthermore, the general anisotropy index (A^U), compression and shear anisotropy percentages (A_B and A_G) correspond to elastic anisotropy [37, 38]. It should be noted that Sb_2Te_3 and Bi_2Te_3 has special

chemical bond and obvious anisotropy in lattice space distribution, which leads to the anisotropy of mechanical and thermoelectric properties. Anisotropy plays important role in Sb_2Te_3 and Bi_2Te_3 films [42, 43], especially in p-type Sb_2Te_3 and n-type Bi_2Te_3 thin films [44].

3.4 Band gap comparison of both single and composite thin films

By constructing superlattice of different structures, different surface states can be obtained. On the basis of studying the factors that can change the surface states, the surface states can be adjusted artificially. The superlattice containing $\text{Sb}_2\text{Te}_3/\text{Bi}_2\text{Te}_3$ film structures are constructed and the energy bands are found to be dependent on the superlattice film structure, shown in Fig. 5.

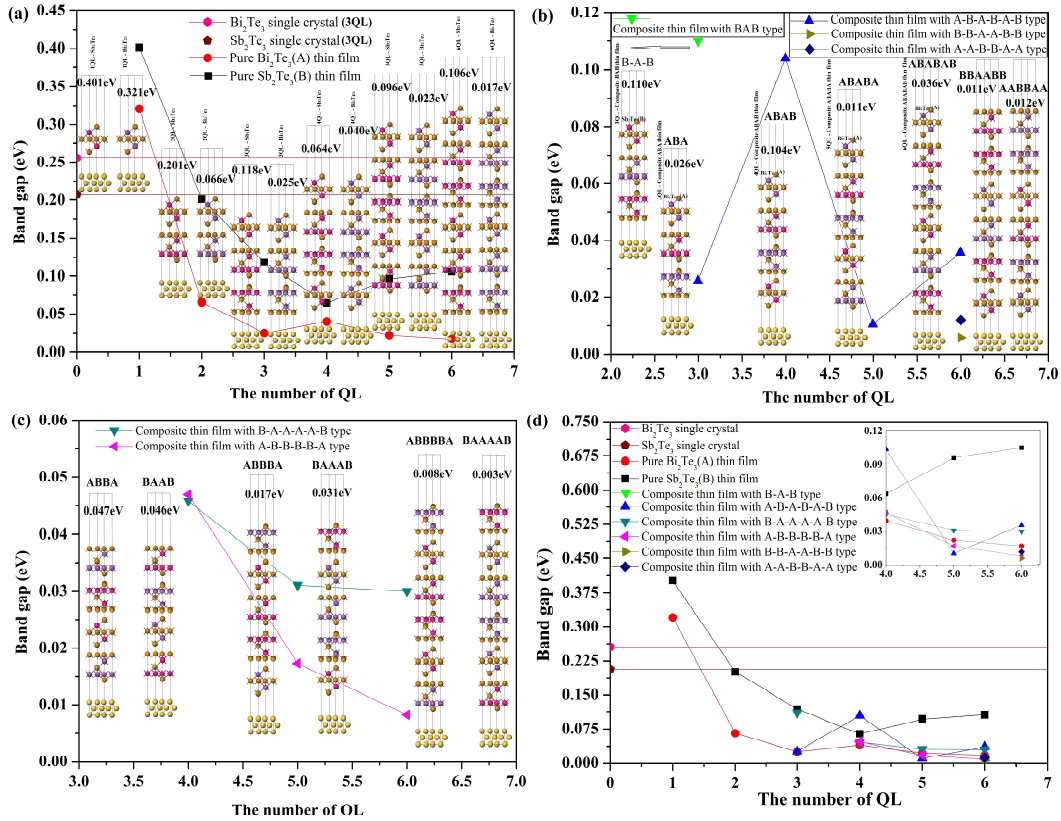


Fig. 5 Comparison of band gap in both single and composite $\text{Sb}_2\text{Te}_3/\text{Bi}_2\text{Te}_3$ thin films

From Fig. 5 that the surface states of the topological insulator films with a superlattice structure can be changed significantly when the crystal unit cell only contains 3QL or 4 QL. As more quintuple layers in the unit cell, the configuration has less impact on the surface state. As in Fig. 5(a), the band gap of pure-phase films decreases to a relatively narrow level with the increase of the layer thickness. From Fig. 5(b)-(c), when the crystal cell contains 3 QL to 4 QL, the influence of the structure of the film on the surface state is obvious. In the case of 3 QL, the surface state gap of the material reaches the room temperature scale if the heavier Bi atomic layer is placed in the outer layer. If the lighter Sb atom layer is placed in the outer layer of the 3QL superlattice, not only the surface state gap is 4 times of the room temperature scale (0.026 eV), but also the time reversal symmetry is destroyed. In the case of 4 QL, the surface state gap of superlattice thin films grown alternately is larger than that of other materials. From Fig. 5(d), when the crystal cell contains 5 QL to 6 QL, the surface energy band properties of the superlattice films have almost reached the room temperature scale, and the influence of the structure of the superlattice films on the surface energy gap is not significant due to the scattering phonons with the thermal conductivity reduced [50, 51].

3.5 Discussion of thermoelectric properties

The calculated C_V of Bi_2Te_3 and Sb_2Te_3 are $123.04 \text{ J}\cdot\text{mol}^{-1}\cdot\text{K}$ and $128.25 \text{ J}\cdot\text{mol}^{-1}\cdot\text{K}$, while the calculated C_p of Bi_2Te_3 and Sb_2Te_3 are $125.85 \text{ J}\cdot\text{mol}^{-1}\cdot\text{K}$ and $131.57 \text{ J}\cdot\text{mol}^{-1}\cdot\text{K}$. The calculated B of Bi_2Te_3 and Sb_2Te_3 are 35.39 GPa and 36.94 GPa . The compressional velocity v_l , the sound velocity v_s and the average sound velocity v_m are separately calculated, which are close to the reference [29] of Sb_2Te_3 and the reference [25] of Bi_2Te_3 . From the comparison of references [14, 15, 46] of Sb_2Te_3 and references [25, 45] of Bi_2Te_3 , Debye temperature θ_D of Sb_2Te_3 is higher than the Bi_2Te_3 . Furthermore, the orientation dependent Grüneisen parameter γ has been extracted by Barron [52] and Cahill [53], namely, $\gamma_{a/c} = [\alpha_{a/c}(C_{11} + C_{12}) + \alpha_{a/c}C_{13}] / C_V$ along the a/c direction. Based on the γ by the Poisson ratio [54] and the Barron-Cahill model, γ of Bi_2Te_3 and Sb_2Te_3 are 1.50 and 1.71. It indicates that the thermal expansion coefficient α rapidly increase from starting and gradually achieve a constant value. For instance, by the equation of $\alpha = 2\alpha_{//} + \alpha_{\perp}$, the α of Bi_2Te_3 and Sb_2Te_3 reaches $4.698 \times 10^{-5} \text{ K}^{-1}$ ($\alpha_{//} = 1.294 \times 10^{-5} \text{ K}^{-1}$, $\alpha_{\perp} = 2.110 \times 10^{-5} \text{ K}^{-1}$) and $6.935 \times 10^{-5} \text{ K}^{-1}$ ($\alpha_{//} = 1.852 \times 10^{-5} \text{ K}^{-1}$, $\alpha_{\perp} = 3.231 \times 10^{-5} \text{ K}^{-1}$) at 275 K, being consistent with the Bi_2Te_3 value of $4.60 \times 10^{-5} \text{ K}^{-1}$ as reported by Feng [9] and the calculated Sb_2Te_3 value of $7.10 \times 10^{-5} \text{ K}^{-1}$ as reported by Bessas [15]. Bi_2Te_3 and Sb_2Te_3 have the average atomic mass of 168.29 amu and 124.64 amu [15], with isothermal compressibility K_T of 2.67 Mbar^{-1} and 3.30 Mbar^{-1} [55]. The calculated lattice thermal conductivities for Sb_2Te_3 and Bi_2Te_3 are $2.38 \text{ W}\cdot\text{m}^{-1}\cdot\text{K}^{-1}$ and $1.56 \text{ W}\cdot\text{m}^{-1}\cdot\text{K}^{-1}$ at 275 K, compared with the κ_{xx} of $1.90 \text{ W}\cdot\text{m}^{-1}\cdot\text{K}^{-1}$ and $1.20 \text{ W}\cdot\text{m}^{-1}\cdot\text{K}^{-1}$ and κ_{zz} of $1.27 \text{ W}\cdot\text{m}^{-1}\cdot\text{K}^{-1}$ and $0.40 \text{ W}\cdot\text{m}^{-1}\cdot\text{K}^{-1}$ for Sb_2Te_3 and Bi_2Te_3 at 300 K [46]. By the equation of $ZT = S^2 \cdot T / \rho \cdot \kappa_T$ [17], the calculated ZT of 0.81 and 0.61 for Sb_2Te_3 and Bi_2Te_3 at 275 K. K_L for all the 60-Å-period structures, no matter the superlattice structure of $30\text{Å}/30\text{Å}$ or $10\text{Å}/50\text{Å}$ or $20\text{Å}/40\text{Å}$, is about $0.25 \text{ W}\cdot\text{m}^{-1}\cdot\text{K}^{-1}$ [17]. Similarly, the calculated total thermal conductivities of the $\text{Sb}_2\text{Te}_3/\text{Bi}_2\text{Te}_3$ superlattice structures with 2QL and 6QL are $0.33 \text{ W}\cdot\text{m}^{-1}\cdot\text{K}^{-1}$ and $0.46 \text{ W}\cdot\text{m}^{-1}\cdot\text{K}^{-1}$, compared to the total thermal conductivity is $0.37 \text{ W}\cdot\text{m}^{-1}\cdot\text{K}^{-1}$ using the same electrical resistivity ρ_{\perp} value of $\sim 1.23 \times 10^{-3} \Omega\cdot\text{cm}$ (along c axis) and $\sim 1.04 \times 10^{-3} \Omega\cdot\text{cm}$ (along a - b axis)[17] and the same S^2T value by the Weidemann–Franz law for determining the ZT value. As the maximum Seebeck coefficient of $\text{Bi}_2\text{Te}_3/\text{Sb}_2\text{Te}_3$ superlattice is $260.00 \mu\text{V}/\text{K}$ [17], using the electrical conductivity σ of $1230 \text{ S}\cdot\text{cm}^{-1}$ [56], the ZT value of the superlattice structures is greatly improved, with the decrease of thermal conductivity from $0.46 \text{ W}\cdot\text{m}^{-1}\cdot\text{K}^{-1}$ to $0.33 \text{ W}\cdot\text{m}^{-1}\cdot\text{K}^{-1}$. The ZT for $\text{Sb}_2\text{Te}_3/\text{Bi}_2\text{Te}_3$ superlattice structures with 2QL and 6QL are 2.69 and 1.93 at 275K, which is close to that of 2.40 at 300K of p-type $10\text{Å}/50\text{Å}$ $\text{Bi}_2\text{Te}_3/\text{Sb}_2\text{Te}_3$ superlattices [17].

4. Conclusion

The electronic structure shows that Bi_2Te_3 (0.256 eV) has the bigger band gap than Sb_2Te_3 (0.207 eV) because of its larger mass (800.80 g/mol). Thus, energy gap can be enlarged with doping heavy elements in compounds for practical applications. For the composite $\text{Bi}_2\text{Te}_3/\text{Sb}_2\text{Te}_3$ structure film, the surface states of the topological insulator films with a superlattice structure are affected by the substrates when the unit cell contains 3 QL, it indicates that we may adjust the surface states by different substrates. With the increase of QL thickness more than 5, because the system energy gap has become stable, the influence of changing the structure of the superlattice film on the energy gap is no longer obvious. The AB-type periodic composite $\text{Bi}_2\text{Te}_3/\text{Sb}_2\text{Te}_3$ film will lead to a large number of point defects in Sb_2Te_3 , thus strongly scattering phonons, and the superlattice can effectively scatter phonons due to its special superlattice structure, resulting in the thermal conductivity significantly reduced **so as to increase the ZT value of the superlattice structures.**

CRedit authorship contribution statement

Jia Fu: Validation, Formal analysis, Resources, Writing - original draft, Visualization, Supervision, Project administration. **Jiaxuan Huang:** Methodology, Data curation. **Fabrice Bernard:** Conceptualization.

Declaration of competing interest

The authors declare that they have no known competing financial interests or personal relationships that could have appeared to influence the work reported in this paper.

Acknowledgements

This paper is supported by the National Natural Science Foundation of China (No: 51905427), National College Students Innovation and Entrepreneurship Training Program (S202010705042), Natural Science Foundation of Shaanxi Province (No. 2020JQ-769) and the Région Bretagne and European Union (CPER-FEDER).

References

- [1] L. Deng, G. M. Chen, Recent progress in tuning polymer oriented microstructures for enhanced thermoelectric performance, *Nano Energy* **80** (2021) 105448.
- [2] H. S. Kim, N. A. Heinz, Z. M. Gibbs, Y. L. Tang, S. D. Kang, G. J. Snyder, High thermoelectric performance in $(\text{Bi}_{0.25}\text{Sb}_{0.75})_2\text{Te}_3$ due to band convergence and improved by carrier concentration control, *Mater. Today* **20** (2017) 452-459.
- [3] H. C. Lv, L. R. Liang, Y. C. Zhang, L. Deng, Z. J. Chen, Z. X. Liu, H. F. Wang, G. M. Chen, A flexible spring-shaped architecture with optimized thermal design for wearable thermoelectric energy harvesting, *Nano Energy* **88** (2021) 106260.
- [4] M. Tan, Y. Deng, Y. Hao, Multilayered structure and enhanced thermoelectric properties of $\text{Bi}_{1.5}\text{Sb}_{0.5}\text{Te}_3$ film with preferential growth, *Phys. Status. Solidi. A* **210** (2013) 2611-2616.
- [5] C. Schumacher, K. G. Reinsberg, R. Rostek, L. Akinsinde, S. Baessler, S. Zastrow, G. Rampelberg, P. Woias, C. Detavernier, J. A. C. Broekaert, J. Bachmann, K. Nielsch, Optimizations of pulsed plated p and n-type Bi_2Te_3 -based ternary compounds by annealing in different ambient atmospheres, *Adv. Energy Mater.* **3** (2013) 95-104.
- [6] J. S. Fan, X. Huang, F. S. Liu, L. Deng, G. M. Chen, Feasibility of using chemically exfoliated SnSe nanobelts in constructing flexible SWCNTs-based composite films for high-performance thermoelectric applications, *Compos. Commun.* **24** (2021) 100612.
- [7] M. Tan, D. Yuan, Y. Wang, Unique hierarchical structure and high thermoelectric properties of antimony telluride pillar arrays, *J. Nanopart. Res.* **14** (2012) 1204.
- [8] Y. C. Lin, J. Liu, F. X. Jiang, An integral p-n connected all-graphene fiber boosting wearable thermoelectric energy harvesting, *Compos. Commun.* **16** (2019) 79-83.
- [9] S. Feng, S. Li, H. Fu, First-principle calculation and quasi-harmonic Debye model prediction for elastic and thermodynamic properties of Bi_2Te_3 , *Comp. Mater. Sci.* **82** (2014) 45-49.
- [10] Y. C. Zhang, L. Deng, H. C. Lv, G. M. Chen, Toward improved trade-off between thermoelectric and mechanical performances in polycarbonate/single-walled carbon nanotube composite films, *NPJ Flex. Electron.* **4** (2020) 26.
- [11] B. L. Huang, M. Kaviani, Ab-initio and molecular dynamics predictions for electron and phonon transport in bismuth telluride, *Phys. Rev. B* **77** (2008) 125209.
- [12] K. Zhao, Y. Wang, C. Xin, Y. Sui, X. Wang, Y. Wang, Z. Liu, B. Li, Pressure-induced anomalies in structure, charge density and transport properties of Bi_2Te_3 : a first principles study, *J. Alloy. Compd.* **661** (2016) 428-434.
- [13] H. C. Chang, C. H. Chen, Y. K. Kuo, Great enhancements in the thermoelectric power factor of BiSbTe nanostructured films with well-ordered interfaces, *Nanoscale* **5** (2013) 7017-7025.
- [14] X. Chen, D. H. Zhou, A. Kiswandhi, I. Miotkowski, Y. P. Chen, P. A. Sharma, A. L. L. Sharma, M. A. Hekmaty, D. Smirnov, Z. Jiang, Thermal expansion coefficients of Bi_2Te_3 and Sb_2Te_3 crystals from 10K to 270K, *Appl. Phys. Lett.* **99** (2011) 261912.
- [15] D. Bessas, I. Sergueev, H. C. Wille, J. Persson, D. Ebling, R. P. Hermann, Lattice dynamics in Bi_2Te_3 and Sb_2Te_3 : Te and Sb density of phonon states, *Phys. Rev. B* **86** (2012) 224301.
- [16] E. Symeou, M. Pervolaraki, C. N. Mihailescu, G. I. Athanasopoulos, C. H. Papageorgiou, T. Kyratsi, J. Giapintzakis, Thermoelectric properties of $\text{Bi}_{0.5}\text{Sb}_{1.5}\text{Te}_3$ thin films grown by pulsed laser deposition, *Appl. Surf. Sci.* **336** (2015) 138-142.
- [17] R. Venkatasubramanian, E. Siivola, T. Colpitts, B. O'Quinn, Thin-film thermoelectric devices with high room-temperature figures of merit, *Nature* **413** (2002) 597-602.
- [18] M. Tan, L. Hao, H. Li, C. Li, X. Liu, D. Yan, T. Yang, Y. Deng, Approaching high-performance of ordered structure Sb_2Te_3 film via unique angular intraplanar grain boundaries, *Sci. Rep.* **10** (2020) 5978
- [19] J. Kim, J. H. Lim, N. V. Myung, Composition- and crystallinity- dependent thermoelectric properties of ternary $\text{Bi}_x\text{Sb}_{2-x}\text{Te}_y$ films, *Appl. Surf. Sci.* **429** (2018) 158-163.
- [20] G. Wang, T. Cagin, Electronic structure of the thermoelectric materials Bi_2Te_3 and Sb_2Te_3 from first-principles calculations, *Phys. Rev. B* **76** (2007) 075201.
- [21] B. L. Huang, M. Kaviani, Ab initio and molecular dynamics predictions for electron and phonon transport in bismuth telluride, *Phys. Rev. B* **77** (2008) 125209.
- [22] J. T. Im, K. T. Hartwig, J. Sharp, Microstructural refinement of cast p-type Bi_2Te_3 - Sb_2Te_3 by equal channel angular extrusion, *Acta Mater.* **52** (2004) 49-55.

- [23] N. Peranio, M. Winkler, D. Bessas, Z. Aabdin, J. König, H. Böttner, R. P. Hermann, O. Eibl, Room-temperature MBE deposition, thermoelectric properties, and advanced structural characterization of binary Bi₂Te₃ and Sb₂Te₃ thin films, *J. Alloy. Compd.* 521 (2012) 163-173.
- [24] X. Feng, C. Hangarter, B. Yoo, Y. Rheem, K. H. Lee, N. V. Myung, Recent progress in electrodeposition of thermoelectric thin films and nanostructures, *Electrochim. Acta* 53 (2008) 8103-8117.
- [25] J. O. Jenkins, J. A. Rayne, R. W. Ure, Elastic moduli and phonon properties of Bi₂Te₃, *Physical Review B*, 5 (1972) 3171-3184.
- [26] Z. Starý, J. Horák, M. Stordeur, M. Stölzer, Antisite defects in Sb_{2-x}Bi_xTe₃ mixed crystals, *J. Phys. Chem. Solids*, 49 (1988) 29-34.
- [27] P. Larson, W. R. L. Lambrecht, Electronic structure and magnetism in Bi₂Te₃, Bi₂Se₃, and Sb₂Te₃ Doped with transition metals (Ti-Zn), *Physical Review B*, 78 (2008) 195-207.
- [28] G. S. Nolas, J. Sharp, J. Goldsmid, *Thermoelectrics: basic principles and new materials developments* [M]. New York: Springer-Verlag Berlin Heidelberg, (2013) 123-131.
- [29] Q. Lu, H. Y. Zhang, Y. Cheng, X. R. Chen, G. F. Ji, Phase transition, elastic and electronic properties of topological insulator Sb₂Te₃ under pressure: first principle study, *Chin. Phys. B* 25 (2016) 026401.
- [30] A. L. Hansen, T. Dankwort, M. Winkler, J. Ditto, D. C. Johnson, J. D. Koenig, K. Bartholomé, L. Kienle, W. Bensch, Synthesis and thermal instability of high-quality Bi₂Te₃/Sb₂Te₃ super lattice thin film thermoelectrics, *Chem. Mater.*, 26 (2014) 6518-6522.
- [31] B. Poudel, Q. Hao, Y. Ma, Y. Lan, A. Minnich, B. Yu, X. Yan, D. Wang, A. Muto, D. Vashaee, X. Chen, J. Liu, M. S Dresselhaus, G. Chen, Z. Ren, High-thermoelectric performance of nanostructured bismuth antimony telluride bulk alloys, *Science*, 320 (2008) 634-638.
- [32] J. Mao, Z. Liu, Z. Ren, Size effect in thermoelectric materials, *NPJ Quantum Mater.*, 1 (2016) 16028.
- [33] H. Jian, T. M. Tritt, Advances in thermoelectric materials research: Looking back and moving forward, *Science*, 357 (2017) eaak9997.
- [34] Y. H. Jia, Q. L. Jiang, B. H. Wang, Z. T. Ma, D. K. Zhao, N. Zheng, J. D. Zhou, P. P. Liu, D. H. Hu, Y. G. Ma, Utilizing perylene diimide as dopant to improve thermoelectric performance of PEDOT:PSS films, *Compos. Commun.* 27 (2021) 100844.
- [35] F. Rieger, V. Roddatis, K. Kaiser, G. Bendt, C. Jooss, Transition into a phonon glass in crystalline thermoelectric (Sb_{1-x}Bi_x)₂Te₃ films, *Phys. Rev. Mater.* 4 (2020) 025402.
- [36] N. W. Park, W. Y. Lee, Y. S. Yoon, G. S. Kim, Y. G. Yoon, S. K. Lee, Achieving out-of-plane thermoelectric figure of merit ZT=1.44 in a p-type Bi₂Te₃/Bi_{0.5}Sb_{1.5}Te₃ superlattice film with low interfacial resistance, *ACS Appl. Mater. Interfaces* 1 (2019) 8247-38254.
- [37] J. Fu, S. Kamali-Bernard, F. Bernard, M. Cornen, Comparison of mechanical properties of C-S-H and Portlandite between nano-indentation experiments and a modelling approach using various simulation techniques, *Compos. part B: Eng.* 151 (2018) 127-138.
- [38] J. Fu, Atomistic simulation of anisotropic crystal structures at nanoscale[M].IntechOpen, 2019.
- [39] J. Jiang, L. Chen, S. Bai, Q. Yao, Q. Wang, Thermoelectric properties of p-type (Bi₂Te₃)_x(Sb₂Te₃)_{1-x} crystals prepared via zone melting, *J. Cryst. Growth*, 277 (2005) 258-263.
- [40] N. H. Trung, K. Sakamoto, N. V. Toan, T. Ono, Synthesis and evaluation of thick films of electrochemically deposited Bi₂Te₃ and Sb₂Te₃ thermoelectric materials, *Materials* 10(2017) 154.
- [41] T. Fang, X. Li, C. Hu, Q. Zhang, J. Yang, W. Zhang, X. Zhao, D. J. Singh, T. Zhu, Complex band structures and lattice dynamics of Bi₂Te₃-based compounds and solid solutions, *Adv. Funct. Mater.* 29 (2019) 1900677.
- [42] J. Kim, M. Zhang, W. Bosze, S. D. Park, J. H. Lim, N. V. Myung, Maximizing thermoelectric properties by nanoinclusion of γ -SbTe in Sb₂Te₃ film via solid-state phase transition from amorphous Sb-Te electrodeposits, *Nano Energy* 13 (2015) 727-734.
- [43] M. S. Dresselhaus, G. Chen, M. Y. Tang, R. G. Yang, H. Lee, D. Z. Wang, Z. F. Ren, J. P. Fleurial, P. Gogna, New directions for low-dimensional thermoelectric materials, *Adv. Mater.* 19 (2007) 1043-1053.
- [44] K. Takayama, M. Takashiri, Multi-layered-stack thermoelectric generators using p-type Sb₂Te₃ and n-type Bi₂Te₃ thin films by radio-frequency magnetron sputtering, *Vacuum* 144 (2017) 164-171.
- [45] L. Pavlova, Y. Shtern, R. Mironov, Thermal expansion of bismuth telluride, *High Temp.* 49 (2011) 369-379.
- [46] T. Fang, X. Li, C. L. Hu, Q. Zhang, J. Yang, W. Q. Zhang, X. B. Zhao, D. J. Singh, T. J. Zhu, Complex band structures and lattice dynamics of Bi₂Te₃-based compounds and solid solutions, *Adv. Funct. Mater.* 29 (2019) 1900677.
- [47] X. L. Shi, J. Zou, Z. G. Chen, Advanced thermoelectric design: from materials and structures to devices, *Chem. Rev.*, 120 (2020) 7399-7515.
- [48] J. F. Li, W. S. Liu, L. D. Zhao, Z. Min, High-performance nanostructured thermoelectric materials, *NPG Asia Mater.* 2 (2010) 152-158.
- [49] J. Fu, F. Bernard, S. Kamali-Bernard, First-principles calculations of typical anisotropic cubic and hexagonal structures and homogenized moduli estimation based on the Y- parameter. Application to CaO, MgO, CH and Calcite CaCO₃, *J. Phys. Chem. Solids* 101 (2017) 74-89.
- [50] M. N. Touzelbaev, P. Zhou, R. Venkatasubramanian, K. E. Goodson, Thermal characterization of Bi₂Te₃/Sb₂Te₃ superlattices, *J. Appl. Phys.* 90 (2001) 763-767.
- [51] S. I. Kim, K. H. Lee, H. A. Mun, H. S. Kim, S. W. Hwang, J. W. Roh, D. J. Yang, W. H. Shin, X. S. Li, Y. H. Lee, G. J. Snyder, S. W. Kim, Dense dislocation arrays embedded in grain boundaries for high-performance bulk thermoelectrics, *Science* 348 (2015) 109-114.
- [52] G. A. Slack. The Thermal Conductivity of Nonmetallic Crystals, *Solid State Phys.* 34 (1979) 1-71.
- [53] D. G. Cahill, S. K. Watson, R. O. Pohl. Lower limit to the thermal conductivity of disordered crystals, *Phys. Rev. B* 46 (1992) 6131-6140.
- [54] T. Jia, C. Gang, Y. Zhang. Lattice thermal conductivity evaluated using elastic properties, *Phys. Rev. B* 95 (2017) 155206.

- [55] N. Sakai, T. Kajiwara, K. Takemura, S. Minomura, Y. Fujii. Pressure-induced phase transition in Sb_2Te_3 , *Solid State Commun.* 40 (1981) 1045-1047.
- [56] Z. Wei, D. Yuan, W. Yao, B. Luo, L. Cao. Preferential growth transformation of $\text{Bi}_{0.5}\text{Sb}_{1.5}\text{Te}_3$ films induced by facile post-annealing process: Enhanced thermoelectric performance with layered structure, *Thin Solid Films*, 556 (2014) 270-276.

